IOP PUBLISHING PHYSICS IN MEDICINE AND BIOLOGY

Phys. Med. Biol. **53** (2008) 505–513 doi:10.1088/0031-9155/53/2/015

High-resolution 3D isotropic MR imaging of mouse flank tumours obtained *in vivo* with solenoid RF micro-coil

W M Holmes[1], S Maclellan[2,3], B Condon[1], C Dufès[4], T R J Evans[5], I F Uchegbu[2] and A G Schätzlein[2]

[1] Division of Clinical Neuroscience, University of Glasgow, Glasgow, UK
[2] The Doctoral Training Centre, Bioengineering Unit, University of Strathclyde, UK
[3] The School of Pharmacy, University of London, London, UK
[4] Strathclyde Institute of Pharmacy and Biomedical Sciences, University of Strathclyde, Glasgow, UK
[5] Centre for Oncology and Applied Pharmacology, Beatson Laboratories, University of Glasgow, Glasgow, UK

E-mail: W.Holmes@clinmed.gla.ac.uk

Received 12 September 2007, in final form 15 November 2007
Published 28 December 2007
Online at stacks.iop.org/PMB/53/505

Abstract

The investigation of mouse flank tumours by magnetic resonance imaging (MRI) is limited by the achievable spatial resolution, which is generally limited by the critical problem of signal-to-noise ratio. Sensitivity was improved by using an optimized solenoid RF micro-coil, built into the animal cradle. This simple design did not require extensive RF engineering expertise to construct, yet allowed high-resolution 3D isotropic imaging at $60 \times 60 \times 60\ \mu m^3$ for a flank tumour *in vivo*, revealing the heterogeneous internal structure of the tumour. It also allowed dynamic contrast enhanced (DCE) experiments and angiography (MRA) to be performed at $100 \times 100 \times 100\ \mu m^3$ resolution. The DCE experiments provided an excellent example of the diffusive spreading of contrast agent into less vascularized tumour tissue. This work is the first step in using high-resolution 3D isotropic MR to study transport in mouse flank tumours.

Introduction

The investigation of animal models using MRI allows non-invasive access to functional, anatomical and physiological information. An inherent problem with studying small animals, e.g. mice, is the greatly reduced size of anatomical structures which necessitates the use of high spatial resolutions. The spatial resolution is generally not limited by the gradient encoding power of the imager but rather by the critical signal-to-noise ratio.

 © 2008 Institute of Physics and Engineering in Medicine

Previous MRI studies of mouse flank tumours have mainly used either whole mouse volume resonators or surface coils. Volume resonators have the advantage of good B1 homogeneity, with the disadvantage of having a very low effective filling factor (tumour size of ∼4 mm, with regard to resonator size of ∼35 mm diameter). The resolution achieved with a mouse volume resonator typically ranges up to 200 × 200 μm^2 with 1–2 mm slice thickness (Kiessling *et al* 2005, Graff *et al* 2005, Yankeelov *et al* 2006).

Of course the signal to noise can be improved by signal averaging, but for *in vivo* studies the duration an animal can be anaesthetized is limited, and long durations are not desirable. Also, in experiments such as dynamic contrast enhanced (DCE) MRI the temporal resolution of scans is important; therefore, this is not usually a significant option.

Other ways to improve signal-to-noise ratio include working at higher magnetic fields or improving the sensitivity of the NMR signal detection, for example by the use of phased array coils or cyro-cooled coils. Recently, a transmit–receive super-conducting surface coil (Ginefri *et al* 2005) has been developed, which for mouse tumours achieved resolutions up to 59 × 59 μm^2 with 300 μm slice thickness, at 1.5 T.

A simpler and often overlooked alternative to these options is to fully optimize the geometry and type of RF coil to suit the sample/region of interest. In the case of *in vivo* imaging of flank tumours on mice, these tumours are small (∼2–5 mm diameter) and protrude out from the side of the animal (∼3–4 mm). The best filling factor possible would be achieved by placing the flank tumour fully inside an RF coil of a slightly larger diameter, with the tumour as far as possible contained within the coil. With the animal lying head to foot inside the magnet (parallel to the B0 field), this would require the axis of the RF coil be perpendicular to the axis of the B0 field. The fundamentals of NMR require that the B1 field, produced by the RF coil, be perpendicular to the B0 magnetic field. Therefore, the ideal coil geometry would be a solenoid, as the B1 field of a solenoid runs along its axis.

The choice of a solenoid has many natural advantages. First, the solenoid is the coil design that allows for the best NMR sensitivity (Mispelter *et al* 2006). For example, compared to a saddle coil of the same dimensions, the sensitivity performance of a solenoid is approximately three times greater (Hoult and Richards 1976). Indeed solenoids are widely used in solid state NMR, where sample loading is not an issue and NMR sensitivity is paramount. Also, small diameter solenoids are simple to construct, and produce high B1 homogeneity (Hoult and Richards 1976). The practical size of an RF solenoid coil is limited by the need for the total length of conductor to be small compared to the wavelength of RF radiation used, otherwise phase differences between different parts of the coil lead to interference of B1 contributions. At high frequency this limits the use of solenoid RF coils to very small diameters.

This paper describes the use of a solenoid micro-coil design that has been optimized for imaging mouse flank tumours *in vivo*. The simple design does not require extensive RF engineering expertise to construct and implement, yet can greatly improve sensitivity and hence spatial and/or temporal resolution.

Material and methods

Solenoid coil and animal cradle

The high sensitivity of a small diameter solenoid required that it be constructed as an integral part of a purpose-built animal cradle, to provide it with mechanical stability (see figure 1). The top of the cradle consists of a thin flat platform, with a hole at the centre, entering to a hollow cylinder (inner diameter 5.5 mm and outer diameter 7.0 mm). Underneath the top platform, the solenoid coil was wound around the outside of the cylinder. This allows the mouse to

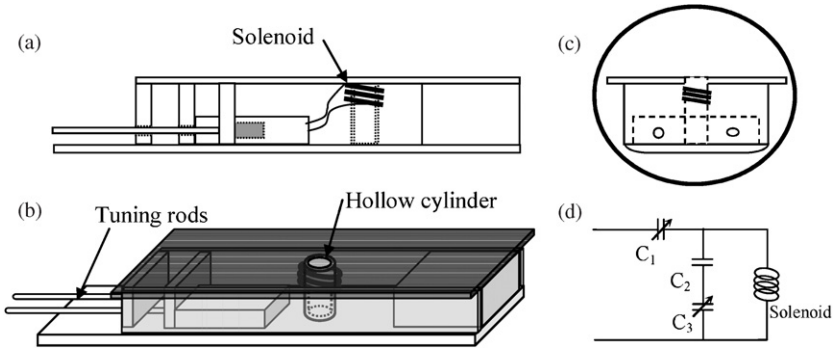

Figure 1. Diagram of animal cradle with built-in solenoid RF coil. (a) Side view. (b) Perspective view. (c) End view of cradle showing how it fits into 60 mm diameter of the micro-imaging gradient set. (d) Resonant circuit design.

be lain on the platform, with the flank tumour placed carefully inside the cylinder, hence inside the solenoid coil. Anaesthetic was administered via a face mask and the animal's body temperature maintained with a close-fitting water jacket. The cradle with a mouse and water jacket in position was designed to fit inside the 60 mm inner diameter of the micro-imaging gradient set (Bruker, BG-6).

The solenoid coil was constructed of 0.8 mm diameter susceptibility matched wire (aluminium core coated with copper), which has lower magnetic susceptibility than copper alone (Haase *et al* 2000). This wire is commonly used in solid-state NMR spectrometers to reduce distortion of the B0 field. The solenoid coil has an inner diameter of 7 mm and is 5 mm in height with two and a half turns, which is close to the optimal design for a solenoid coil (Haase *et al* 2000). The total length of the conductor was 55 mm, compared to a RF wavelength of 999 mm at 300 MHz, thereby obeying the rule of thumb set out by Chen and Hoult (1989) for a solenoid coil to have good B1 homogeneity.

Figure 1(d) shows the RF circuit design used (Mispelter *et al* 2006, Fukushima and Roeder 1981). This consists of two variable air capacitors (C1 and C3) of 0.6 pF to 6.0 pF (Johanson), accessed by tuning rods. C3 is a 1.8 pF ceramic chip capacitor (Temex). The solenoid coil was operated in transmit/receive mode using the standard scanner electronics. Unlike a receive-only coil this mode does not require active decoupling, thus greatly simplifying construction.

Animal preparation

Imaging was performed on female mice (CD1-nu, mean weight 20 g) with established A431 epidermoid carcinoma xenografts of around 5 mm diameter (ATCC CRL-1555). The mice were anaesthetized using 2–3% isofluorane, in a 70/30 mixture of nitrous and oxygen, applied via a face mask. The body temperature was maintained at 37 °C, using a water jacket. Temperature, respiration and ECG were monitored using a BIOPAC system (Goleta, CA, USA). A bolus of contrast agent was manually administered intravenously via a tail vein cannulation. The contrast agent (Magnevist, Schering, Germany) was used at a dose of 1.0 mmol Gd kg^{-1} body weight.

MR imaging

Imaging was performed on a Bruker Biospec Avance system using a 7T horizontal 30 cm bore magnet. A Bruker micro-imaging gradient insert (BG-6), inner diameter 60 mm, was

used, with 100 A amplifiers, giving a maximum gradient of 1000 mT m^{-1} with a rise time of 50 μs.

In vivo high spatial resolution (HSR) images were acquired using a T1 weighted 3D FLASH gradient echo sequence with the following parameters: isotropic pixels 60 × 60 × 60 μm^3, field of view 7.7 × 6.0 × 6.0 mm^3 and an acquisition matrix of 128 × 100 × 100. The sequence used an echo time of 3.5 ms and a recovery time of 100 ms, a bandwidth of 50 kHz and a flip angle of 30°. Total scan time of 50 min.

In order to image the slow flow in the tumour vessels a multi-slice 2D flow compensated gradient echo sequence was used, with the slices perpendicular to the axis of the coil. Isotropic voxels were acquired with 100 × 100 μm^2 in-plane resolution and 60 sequential slices of 100 μm thickness. The increased rate of replacement of blood in these thin slices helps to resolve slow flowing vessels. The echo time used was 5 ms and the recovery time was 40 ms with a bandwidth of 50 kHz and 8 averages. Total scan time was 22 min.

In vivo DCE imaging of flank tumours was performed using a 3D FLASH sequence with the following parameters: isotropic voxels 100 × 100 × 100 μm^3, field of view 8 × 8 × 8 mm^3 and an acquisition matrix of 80 × 80 × 80. This sequence used an echo time of 3.5 ms and a recovery time of 25 ms, a bandwidth of 50 KHz and a flip angle of 30°. Images were acquired immediately before and every 10 min post injection. As the tumour is mainly contained within the coil, a much reduced FOV can be used, helping to reduce the scan time. Placing the read direction along the coil axis removes the problem of signal from the body of the mouse folding back in to the image. The same sequence parameters were also used to image a phantom in order to assess the image homogeneity of the coil.

Results

Figure 2 shows gradient echo images acquired with a cylindrical phantom of aqueous copper sulfate, illustrating good image homogeneity. The profiles of normalized signal intensity are also shown, relative to the cradle position. The calculated uniformities, within 10% of the minimum or maximum, were 3.7 mm perpendicular and 2.7 mm parallel to the axis of the coil, as used by Alecci *et al* (2003) and Giovannetti *et al* (2004). The Q factor was measured as the ratio of the resonant frequency to the frequency bandwidth at −3 dB, using a network analyser (Agilent 8712ET), with the coil tuned and matched to 300 MHz and 50 Ω. The −3 dB bandwidth was located at 3 dB below the reference level (Fan *et al* 2006). The loaded and unloaded Q factor of the phantom was measured as 118 and 129.

An example of a high-resolution scan of a mouse flank tumour, measured using the solenoid coil, is shown in figure 3. This 3D dataset has isotropic pixel resolution of 60 × 60 × 60 μm^3. At this high resolution the 3D heterogeneous structure of the tumour is apparent. It is easy to identify tumoural tissue, normal tissue and the rim of the tumour. Such high-resolution images reveal structures at a histological scale and can be used to monitor and study tumour development and response to therapy in preclinical development.

The DCE experiment was performed with manual intravenous injection of a bolus of contrast agent. Figure 4(a) shows a cross-section through the centre of the 3D dataset of the tumour. Following injection of contrast agent there is a rapid signal enhancement at the tumour rim. The contrast agent can then be seen to be transported radially into the tumour tissue, before being washed out. Figure 4(c) shows the signal profile of a line through the centre of the tumour, which clearly shows the radial spreading of contrast agent into the tumour. The traditional way of analysing DCE data is via time profile plots of signal or concentration. Figure 4(d) shows such plots taken from different points in the tumour.

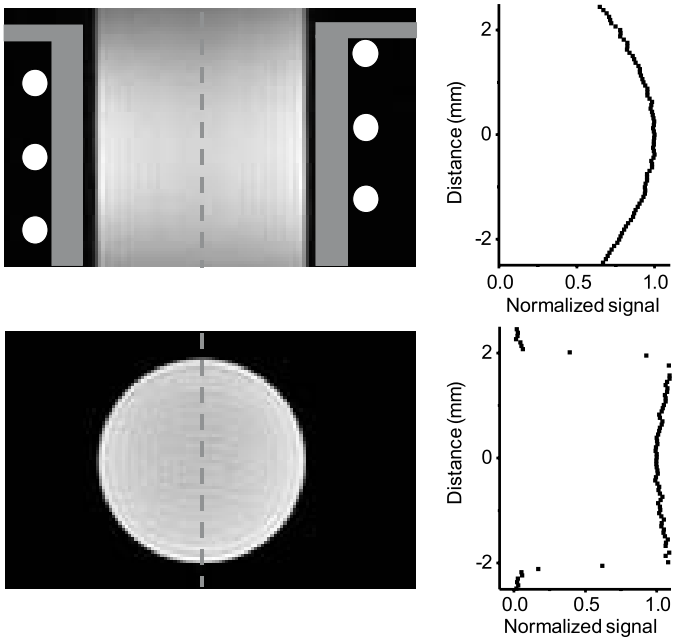

Figure 2. Gradient echo images obtained of phantom of aqueous copper sulfate. (a) Vertical image showing the position of the solenoid coil and the animal platform. (b) Vertical signal profiles through phantom. (c) Horizontal image through centre of coil. (d) Horizontal signal profile through phantom. Imaged using 3D FLASH sequence: Te 3.5 ms, Tr 25 ms, flip-angle 30°, isotropic voxels $100 \times 100 \times 100$ μm^3, field of view $8 \times 8 \times 8$ mm^3, matrix of $80 \times 80 \times 80$. Solutions T1 = 86.7 ms and T2 = 74 ms.

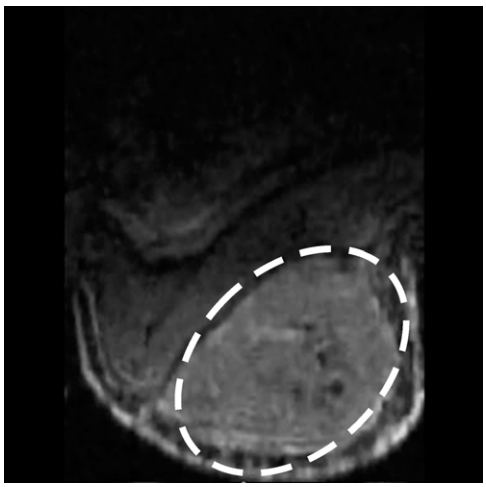

Figure 3. A 3D isotropic $60 \times 60 \times 60$ μm^3 T1 weighted high-resolution scan of mouse flank tumour. The field of view of the above image is 7.7×7.7 mm^2. The dotted ellipse indicates the location of the tumour tissue.

In order to better understand the role of vascular delivery of the contrast agent in this process, a high-resolution angiography sequence was used to identify vessels in the tumour.

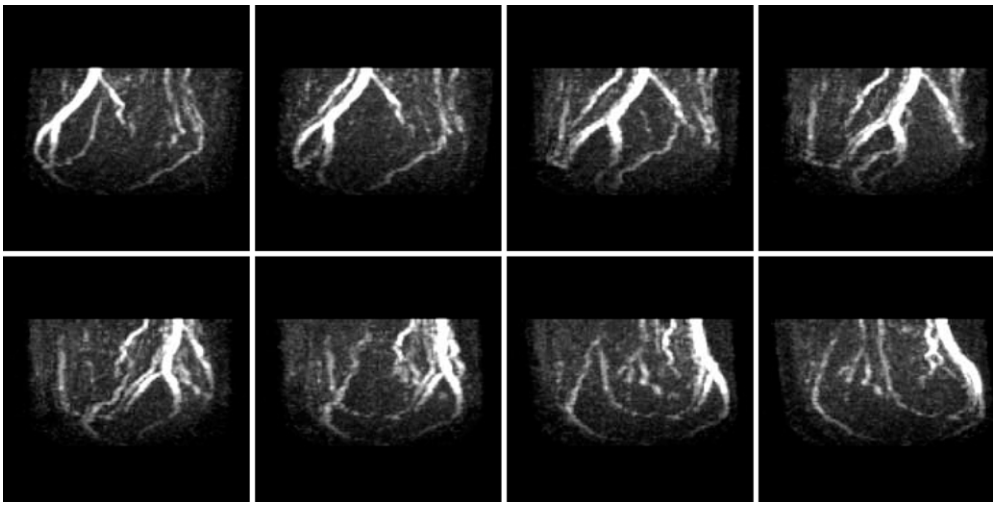

Figure 4. A 3D isotropic 100 × 100 × 100 μm^3 angiogram of mouse flank tumour, displayed as a maximum intensity projection (MIP). The MIP is rotated in 24° steps to highlight the 3D 'claw' like structure of vessels.

Figure 5 shows images from a 3D high resolution (100 × 100 × 100 μm^3) maximum intensity projection (MIP) angiograghy of a mouse flank tumour. Large and small vessels are visible in a 'claw' like encompassment of the tumour.

Discussion

There is an increasing appreciation of the role of spatiotemporal heterogeneity of tumours in cancer therapy (Jain 1990). Even for the low molecular weight drugs currently dominating clinical practice the relevance of this heterogeneity has been demonstrated convincingly in the clinic: Lankelma and colleagues demonstrated that in breast cancer variations in cancer cell density can lead to heterogeneity of drug distribution, i.e. doxorubicin had not reached denser areas of breast tumours even 24 h after therapeutic administration making it likely that potentially sub therapeutic drug levels may be linked to drug resistance and therapeutic failure (Lankelma *et al* 1999). As transport in tumours is typically diffusion limited such barriers would be expected to potentially affect higher MW agents such as antibodies or nanomedicines significantly more (Cassidy and Schätzlein 2004). We believe that isotropic high-resolution three-dimensional imaging of transport process in tumours can help to better understand the role of heterogeneity for the transport of therapies in the tumour.

Typically, DCE MRI experiments on mouse flank tumours are performed using high in-plane resolution images, with a large slice thickness (typically, 200 × 200 μm^2, with 1–2 mm slice thickness). This gives a false sense of resolution, because of course any heterogeneity is averaged over the whole of the slice direction. The DCE data shown in figure 4 improves on this by imaging using 100 × 100 × 100 μm^3 isotropic voxels, allowing high-resolution three-dimensional imaging of transport processes within the tumour.

MR angiography has been previously used to characterize intratumoural vasculature in mice (Fink *et al* 2003) and correlations made with histology (Graff *et al* 2005). Though, with a spatial resolution of 166 × 206 × 329 μm^3, only larger vessels could be visualized. Such tumour angiography, as demonstrated in this paper, with resolution of 100 × 100 ×

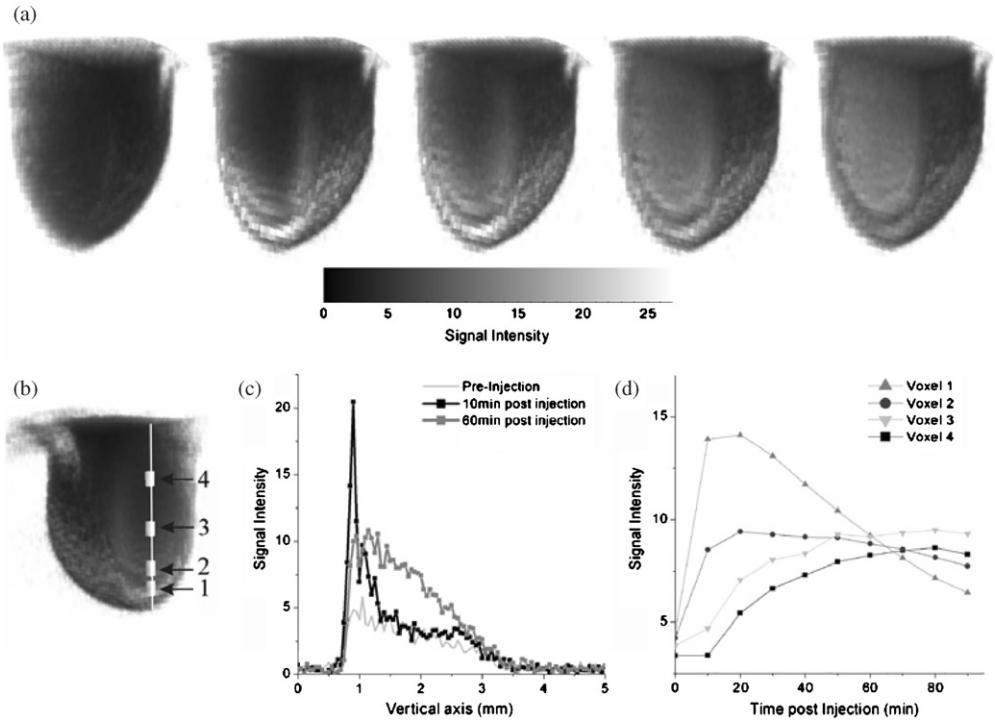

Figure 5. *In vivo* 3D isotopic datasets of mouse flank tumour, voxel size 100 × 100 × 100 μm^3. (a) Cross-section through 3D dataset pre- and 10 min, 20 min, 40 min, 60 min post-injection. Radial diffusion of contrast agent into tumour is apparent. (b) Position of voxels and line profile. (c) Line profile of signal intensity. (d) Time course of signal taken at selected locations.

100 μm^3, identical to that of the DCE data, is better able to detect much smaller vessels (figure 5), in this case highlighting the claw-like encompassment of the tumour. This could potentially allow serial observations of anti-vascular effects caused by vascular disrupting agents (VDA) (Siemanns *et al* 2004).

Currently, the most commonly used method for the measurement of therapeutic response in preclinical development is the determination of the volume of subcutaneously inoculated tumours in mice based on calliper measurements. While having the advantage of simplicity this is prone to error due to the approximation of tumour shape to an ellipsoid (Cornelissen *et al* 2005). It is common to use MRI 3D based volumetry to size human tumours. Recently, this has been applied to sizing mouse tumours, though using a low spatial resolution (500 × 1000 × 1000 μm^3) (Cornelissen *et al* 2005). Using high-resolution isotopic MRI images, such as presented in this paper, would greatly improve the accuracy of serial tumour volume measurements in mice. Furthermore, there is an increasing need to develop methods that allow monitoring of early responses which may not immediately translate into substantial tumour volume changes and to relate these to tumour structure and histology.

The DCE data shown in figure 4 are worthy of further comment, as the high-resolution 3D dataset shows slow radial spreading of contrast agent from regions of high-to-low concentration, i.e. from the well-vascularized periphery, towards the centre of the tumour. This suggests that as well as perfusion, the process of Fickian diffusion may also contribute to transport. The ability to monitor such process is of potential therapeutic relevance given that

transport in the tumour is likely to be diffusion limited due to the reduction of perfusion and convective transport brought about through the increased interstitial fluid pressure (IFP) in the tumour (Minchinton and Tannock 2006). To assess this, an estimate is needed of the possible displacement of contrast agent due to diffusion over the duration of the experiment. This requires knowledge of the apparent diffusion coefficient (ADC) of magnevist, D_{m} within the tumour tissue. Although this value has not yet been experimentally determined, an estimate can be made from other literature data. Osuga and Han (2004) have given an approximate value for the diffusion coefficient of magnevist in water as $0.4 \times 10^{-9}\ \mathrm{m^2\ s^{-1}}$, and the self-diffusion coefficient of water is known to be $2.1 \times 10^{-9}\ \mathrm{m^2\ s^{-1}}$. In tumour tissue the apparent diffusion coefficient (ADC) of water molecules is reduced to between 0.6 and $1.0 \times 10^{-9}\ \mathrm{m^2\ s^{-1}}$ (Herneth *et al* 2003). We therefore estimate D_{m} to be approximately 0.1 to $0.2 \times 10^{-9}\ \mathrm{m^2\ s^{-1}}$. Giving magnevist a root-mean-squared displacement, x_{rms}, in 60 minutes of between 1.4 mm and 2 mm (using $x_{\mathrm{rms}} = \sqrt{6 D_m t}$). This is approximately the same length scale as the spreading seen in figures 4(a) and (c), i.e. over tens of voxels, suggesting the possibility of Fickian diffusion as an additional transport mechanism. Currently, DCE time courses of individual voxels, such as shown in figure 4(d), are modelled using compartmental models of perfusion (Tofts and Kermode 1989, Tofts 2003). These models consider perfusion in each voxel in isolation, and assume no transport of contrast agent occurs between neighbouring voxels over time. Fickian diffusion of contrast agent across voxels would violate this assumption, leading to inaccurate model predictions.

Conclusion

This paper has described the use of a simple solenoid micro-imaging coil for *in vivo* imaging of cancerous flank tumours on mice. The solenoid being the optimal geometry for this situation, giving good B1 homogeneity and high sensitivity. The improved sensitivity allowed high-resolution isotropic imaging of up to $60 \times 60 \times 60\ \mu\mathrm{m}^3$ of *in vivo* flank tumours, which is currently the highest resolution demonstrated in the literature. The high-spatial resolution clearly revealed the 3D heterogeneity of the tumour.

The coil has also been used to obtain isotropic 3D MRI DCE experiments ($100 \times 100 \times 100\ \mu\mathrm{m}^3$) and MR angiography ($100 \times 100 \times 100\ \mu\mathrm{m}^3$) of mice flank tumours *in vivo*. The angiograph showed large and small vessels in a 'claw' like encompassment of the tumour. The DCE dataset clearly demonstrated the slow transport of contrast agent radially into the poorly vascularized centre of the tumour, from the better vascularized outer rim and highlighted the extensive heterogeneity of transport within the tumour.

Acknowledgments

This research was supported by Tenovus Scotland, Cancer Research UK (AGS) and a EPSRC studentship (SM).

References

Alecci M, Collins C M, Wilson J, Wanzhan L, Smith M B and Jezzard P 2003 Theoretical and experimental evaluation of detached endcaps for 3T birdcage coils *Magn. Reson. Med.* **49** 363–70

Cassidy J and Schätzlein A G 2004 Tumour targeted drug and gene delivery: principles and concepts *Expert Rev. Mol. Med.* **6** 1–17

Chen C N and Hoult D I 1989 *Biomedicial Magnetic Resonance Technology* (Bristol: Adam Hilger)

Cornelissen B, Kersemans V, Jans L, Staelens L, Oltenfreiter R, Thonissen T, Achten E and Slegers G 2005 Comparison between 1 T MRI and non-MRI based volumetry in inoculated tumours in mice *Br. J. Radiol.* **78** 338–42

Fan X, Markiewicz E J, Zamora M, Karczmar G S and Roman B B 2006 Comparison and evaluation of mouse cardiac MRI acquired with open birdcage, single loop surface coil and volume birdcage coils *Phys. Med. Biol.* **51** 451–9

Fink C, Fabian K, Bock M, Lichy M P, Misselwitz B, Peschke P, Fusenig N E, Grobholz R and Delorme S 2003 High-resolution three Dimensional MR angiography of rodent tumors: morphologic characterization of intratumoral vasculature *J. Magn. Reson. Imaging* **18** 59–65

Fukushima E and Roeder S B W 1981 *Experimental Pulse NMR: A Nuts and Bolts Approach* (Reading, MA: Perseus)

Ginefri J C, Poirier-Quinot M, Robert P and Darrasse L 2005 Contrast-enhanced dynamic MRI protocol with improved spatial and time resolution for *in vivo* microimaging of the mouse with a 1.5-T body scanner and a superconducting surface coil *Magn. Reson. Imaging* **23** 239–43

Giovannetti G, Francesconi R, Landini L, Santarelli M F, Positano V, Viti V and Benassi A 2004 Conductor geometry and capacitor quality for performance optimisation of low-frequency birdcage coils *Concepts Magn. Reson.* B **20** 9–16

Graff B A, Benjaminsen I C, Brurberg K G, Ruud E M and Rofstad E K 2005 Comparison of tumor blood perfusion assessed by dynamic contrast enhanced MRI with tumour blood supply assessed by invasive imaging *J. Magn. Reson. Imaging* **21** 272–81

Haase A *et al* 2000 NMR probeheads for *in vivo* applications *Concepts Magn. Reson.* **12** 361–88

Herneth A M, Guccione S and Bednarski M 2003 Apparent diffusion coefficient: a quantitative parameter for *in vivo* tumor characterisation *Eur. J. Radiol.* **45** 208–13

Hoult D I and Richards R E 1976 The signal-to-nosie ratio of the nuclear magnetic resonance experiment *J. Magn. Reson.* **24** 71–85

Jain R K 1990 Physiological barriers to delivery of monoclonal antibodies and other macromolecules in tumors *Cancer Res.* **50** 814s-819s

Kiessling F, Le-Huu M, Kunert T, Thorn M, Vosseler S, Schmidt K, Hoffend J, Meinzer H P, Fusenig N E and Semmler W 2005 Improved correlation of histological data with DCE MRI parameter maps by 3D reconstruction, reslicing and parameterization of histological images *Eur. Radiol.* **15** 1079–86

Lankelma J, Dekker H, Luque R F, Luykx S, Hoekman K, van der Valk P, van Diest P J and Pinedo H M 1999 Doxorubicin gradients in human breast cancer *Clin. Cancer Res.* **5** 1703–7

Minchinton A I and Tannock I F 2006 Drug penetration in solid tumors *Nat. Rev. Cancer* **6** 563

Mispelter J, Mihaela L and Briguet A 2006 *NMR Probeheads for Biophysical and Biomedical Experiments* (London: Imperial College Press)

Osuga T and Han S 2004 Proton magnetic resonance imaging of diffusion of high and low molecular weight contrast agents in opaque porous media saturated with water *Magn. Reson. Imaging* **22** 1039–42

Siemanns D W, Chaplin D J and Horsman M R 2004 Vascular targeting therapies for treatment of malignant disease *Cancer* **100** 2491–9

Tofts P S 2003 *Quantitative MRI of the Brain* (Chichester: Wiley) pp 341–60

Tofts P S and Kermode A G 1989 Measurement of blood-brain barrier permeability and leakage space using dynamic MR imaging *Magn. Reson. Med.* **17** 357–67

Yankeelov T E, DeBusk L M, Billheimer D D, Luci J J, Lin P C, Price R R and Gore J C 2006 Repeatability of a reference region model for analysis of murine DCE-MRI data at 7T *J. Magn. Reson. Imaging* **24** 1140–7